Available online at www.sciencedirect.com
ScienceDirect
Carbohydrate Polymers 68 (2007) 329–340
Carbohydrate Polymers
www.elsevier.com/locate/carbpol

X-ray tomography study of the cellular structure of extruded starches and its relations with expansion phenomenon and foam mechanical properties

P. Babin [a,c], G. Della Valle [b,*], R. Dendievel [a], D. Lourdin [b], L. Salvo [a]

[a] *Génie Physique et Mécanique des Matériaux – INPG, BP46 38402 St. Martin d'Hères, France*
[b] *Unité de Recherches sur les Biopolymères, Interactions et Assemblages (BIA), INRA, Rue de la Géraudière, BP 71627, 44316 Nantes Cedex 03, France*
[c] *Sciences Computer Consultants, Parc de la Richelandière, 42000 St. Etienne, France*

Received 31 July 2006; received in revised form 27 November 2006; accepted 1 December 2006
Available online 22 January 2007

Abstract

The cellular structure of extruded starch foams, with different amylose content (0–70%) has been determined by X-ray tomography (10 and 40 μm), leading to highly contrasted 3D images. These foam structures were analysed using a 3D granulometric approach. Their cellular features were determined for relative density (D^*) values in the interval [0.11, 0.34]. Their mean cell size (MCS) and mean cell wall thickness (MWT) varied in the range [0.2, 5 mm] and [75, 630 μm], respectively, and were strongly correlated. For the same value of D^*, the finest structures (MCS < 2 mm and MWT < 300 μm) were found the most resistant to rupture. These finest cellular structures were mainly obtained for larger moisture content (24%) during extrusion. The influence of the extrusion variables on the phenomena occurring at die expansion, such as nucleation, bubble growth and coalescence, was discussed. Finally, the influence of amylose content was attributed to elongational viscosity, in relation with the storage modulus in the rubbery domain.

Keywords: Amylose; Cell size; Glass transition temperature; Image analysis; Melt viscosity; Stress at rupture

1. Introduction

The texture of manufactured foods is related to their mechanical properties which in turn depends on their structure and the way it has been generated during processing. This is also the case for solid food foams, among which cereal products are particularly relevant.

In the case of cellular solids, either food materials or industrial foams, mechanical properties, such as Young Modulus and stress at rupture, can be related to the relative density $D^* = \rho^*/\rho_s$ by power laws, where ρ^* is the density of the cellular solid and ρ_s that of the cell wall material (Gibson & Ashby, 1997). But, in the case of solid food foams, even model products like extruded starchy materials, discrepancy on exponent value of the power law and a lack of fit of experimental data to the power law are often encountered, although relevance of Gibson & Ashby's model is admitted (Hayter, Smith, & Richmond, 1986; Liu, Chuah, & Scanlon, 2003; Lourdin, Della Valle, & Colonna, 1995; Warburton, Donald, & Smith, 1990). Liu and Scanlon (2003) proposed to improve this fitting by integrating the fractal dimension of the solid foam in order to take into account the macroscopic length of the foam sample. Additional microstructural characteristics, such as cell size heterogeneity, have recently been shown of significant effect on the mechanical behaviour of solid foams predicted by finite element modeling (Fazekas, Dendievel, Salvo, & Brechet, 2002).

In spite of their importance, and due to experimental constraints, 3D microscopic cell expansion (mean cell size, cell size heterogeneity) and morphology (shape, sphericity,

* Corresponding author. Tel.: +33 2 40 67 50 00; fax: +33 2 40 67 50 06.
E-mail address: dellaval@nantes.inra.fr (G. Della Valle).

0144-8617/$ - see front matter © 2006 Elsevier Ltd. All rights reserved.
doi:10.1016/j.carbpol.2006.12.005

orientation, anisotropy), have hardly been quantitatively described. Warburton et al. (1990) provided a quantitative 2D description of starch extrudates sections observed by optical microscopy. They later improved their qualitative description by scanning electron microscopy allowing to map the extrusion conditions leading to the polyhedral or spherical shapes of extrudates cells (Warburton, Donald, & Smith, 1992). They also suggested that the difference between product and glass transition temperature ($T_p - T_g$) would play an essential role in the shape of cells and consequently in the density. Meanwhile, during polystyrene processing for microcellular foams, Park, Behravesh, and Venter (1998) found that CO_2 cells undergo coalescence for high temperature or for a large difference between polymer and die temperatures. This result was interpreted by a poor elongational resistance of the polymer melt at high temperature rather than by a larger value of ($T_p - T_g$). Finally, concerning foam extrusion of synthetic polymers, there is a general agreement to consider that a high pressure drop at the die leads to a greater number of cells and a concomitant decrease of cell size (Gendron, Huneault, Tatibouët, & Vachon, 2002; Han, Koelling, Tomasko, & Lee, 2002; Lee, 2001).

Such results are not available for starch foams extrusion. The results obtained by Della Valle, Vergnes, Colonna, and Patria (1997) on starch with different amylose content completed the statements of Kokini, Chang, and Lai (1992) on the influence of shear viscosity of molten starches on the macroscopic expansion behaviour. They also suggested that ($T_p - T_g$) determined the final collapse of the extrudate. For maize grits, Desrumaux, Bouvier, and Burri (1998) have proposed that, for the same density, two cellular structures, either coarse or fine, may be obtained, according to the main mechanism of expansion, radial or axial, respectively, depending on extrusion conditions. A deeper knowledge of the cellular structure of the extruded foams would also provide the numerical simulation studies of bubble growth (Alavi, Rizvi, & Harriott, 2003; Fan, Mitchell, & Blanshard, 1994) with the necessary data for their validation in the same way as for the study of bubble growth in polystyrene melt (Tuladhar & Mackley, 2004).

Either for the mechanical properties or for expansion phenomenon, there is a need to better determine the cellular features of the solid extruded starchy foam, a purpose for which X-ray tomography seems well suited. X-ray tomography is one of the most powerful non destructive techniques which provide direct images of the bulk of heterogeneous materials at the relevant scale. Recently, its interest for food products has been underlined by Whitworth and Alava (2004) for bread processing. Lim and Barigou (2002) also suggested some image analysis procedures to define the microstructural features, and Falcone et al. (2004) applied it to bread before showing how to analyze the images of two samples (Falcone et al., 2005). Trater, Alavi, and Rizvi (2005) confirmed its relevance in the case of extruded foams by applying it to four samples of wheat starch/whey extruded blends. Image analysis was first performed in 2D whereas 3D information was obtained after integration of 2D data for several slices. In the last ten years, the use of synchrotron X-ray radiation, coupled with new detectors, has opened new possibilities. Three-dimensional images of the interior of micro-heterogeneous materials can be obtained with a resolution of a few microns (Maire et al., 2003). More recently, Babin et al. (2006) applied the same technique and 3D image analysis to study the evolution of cellular structure of bread dough during baking. The aim of this work is to determine the cellular structure of extruded starch foams in order to ascertain the links with their mechanical properties and the mechanisms of texture creation by extrusion. Starch extrudates samples with different amylose content and expanded under controlled thermal and flow conditions were studied by X-ray tomography and analysis of the resulting 3D images. Expanded starches samples with same density but displaying different normalized mechanical properties (Lourdin et al., 1995), here stress at rupture, were first selected in this purpose. Other complementary samples were selected in order to take into account the change of processing conditions.

2. Materials and methods

2.1. Materials

Solid food foams were processed by extrusion of four different starches made from high amylose maize (70% amylose), noted A and waxy maize (99% amylopectin), noted D, provided by Roquette (F62-Lestrem), and the two intermediate blends B with 47% amylose and C with 23.5% amylose. Extrusion was achieved on a Clextral BC45 twin-screw extruder (screw diameter 56 mm, screw length 1 m) with various controlled conditions: temperature, added water, feed rate and screws rotation speed according to the experimental procedure detailed by Della Valle, Colonna, Patria, and Vergnes (1996, 1997). Steady-state shear viscosity was measured on a specific slit die rheometer (Rheopac), attached to the die head of the extruder, which allowed to vary locally the shear rate γ without changing the thermomechanical history of the product and thus, to determine the power law for the viscous behaviour of molten starches. The design and processing of the Rheopac system is fully described in Vergnes, Della Valle, and Tayeb (1993).

Twenty samples, among all those processed, were chosen (Table 1) to be studied by X-ray tomography. On the one hand, the samples were chosen so that they have approximately the same density but different mechanical properties. On the other hand, expanded starches with different processing variables (T_p product temperature, MC moisture content, η melt shear viscosity) were selected to highlight the links between the extrusion conditions and the resulting cellular microstructure.

Some of them were reduced to powder by a cryogrinder. Afterwards, powder were hydrated by conditioning

Table 1
Extrusion conditions, (from Della Valle et al., 1997), and results of cellular structure of starch foams with different amylose content (A: 70%, B: 47%, C:23%, D: 0%)

Sample	Extrusion and flow conditions				Density ρ^* (kg/m^3)	Cellular features determined by X-ray tomography		
	MC[a]	T_p[a]	γ (s^{-1})	η (Pa s)		Relative density D^* (kg/m^3)	MWS (μm)	MCS (mm)
A1	0	0	142	224	109	0.11	353	3.8
A2	0	0	26	619	244	0.2	624	3.3
A3	+	0	136	222	144	0.15	80	0.74
A4	+	0	19	760	298	0.34	148	0.58
A5	+	+	162	190	138	0.18	313	1.98
A6	+	+	36	276	262	0.25	85	0.49
A7	+	+	12	486	327	0.34	75	0.22
B1	0	0	111	282	118	0.15	319	2.69
B2	0	0	44	433	202	0.16	94	0.82
B3	0	+	101	254	169	0.13	77	0.72
B4	+	0	68	363	269	0.26	147	0.67
B5	+	0	29	499	359	0.35	143	0.54
B6	+	+	56	278	267	0.23	123	0.84
C1	0	0	55	507	274	0.24	611	3.02
C2	0	+	67	230	270	0.19	133	1.03
C3	0	+	8	626	329	0.3	98	0.35
C4	+	+	130	224	465	0.34	208	0.86
D1	0	−	98	496	262	0.15	553	4.84
D2	0	0	146	291	302	0.21	433	2.8
D3	+	−	116	305	339	0.22	595	3.36

[a] 0 stands for extrusion moisture content MC = 20% (wb) and product temperature at the die $T_p = 163 \pm 3$ °C, (+) 24% and 187 ± 2 °C, respectively, whereas $T_p(-) = 138 \pm 2$ °C.

under 100% relative humidity until a water content of 20% was reached. From hydrated powder, films were obtained by thermomoulding at 120 °C and 200 bar during 10 min. Before mechanical testing, films were stored in an atmosphere controlled by a saturated $MgCl_2$ solution (rh 33% at 25 °C) in order to reach a water content of 9–10%, close to the water content of extruded foams.

2.2. X-ray tomography

The principle of X-ray tomography is based on the difference in material density which is reflected in the different degrees of X-ray absorption. This technique is thus of particular interest in the case of cellular materials since the contrast between void and matter is very strong. In extruded starch samples, for example, X-rays are more strongly absorbed and then attenuated by the cell wall than by the bubbles, thus enabling the two phases to be clearly displayed.

The basic principle, as shown on Fig. 1, consists in targeting the sample with a monochromatic X-ray beam. The X-rays not absorbed by the sample are collected on a specially designed X-ray detector. A projection or radiograph is then obtained displaying the differences in density at each of several thousand pixels of a charge-coupled-device (CCD) camera. A tomographic scan results from the combination of several hundred radiographs, each one taken with a different orientation of the sample, fixed on a rotation stage. The angular step between each projection being very small, it is possible to reconstruct the three-dimensional structure of the sample, using an appropriate mathematical algorithm.

In this study, the X-rays are provided by a synchrotron radiation (the European Synchrotron Radiation Facility, F-38, Grenoble), that enables one to obtain the best quality images in terms of signal-to-noise ratio and a spatial resolution allowing high-resolution tomography. The X-ray beam has a very high intensity and is monochromatic which allows quantitative reconstructions. A 1024 * 1024 CCD camera was used. Each scan took about 10 min and comprised 900 two-dimensional shadow X-ray images.

A cube of each solid specimen was cut using a circular saw for a pixel size, noted SPR, of 10 μm the dimensions of the specimen were (10 mm)^3. For those observed with a 40 μm SPR, dimensions were (40 mm)^3. The resolution was selected by considering the cell size necessary to get a representative volume. The temperature inside the X-ray chamber was close to the room temperature.

2.3. Image analysis

In the following, extrudate images are represented according to the following coordinates: z, flow direction, x vertical (thickness) and y transverse (width) in the die (Fig. 1). The 3D images obtained were 256 grey level (GL) digital images. Image analysis was directly performed on these 3D images using softwares specially developed from ImageJ (http://rsb.info.nih.gov/ij/) and Aphelion (ADCIS-SA, 14-France). A volume of interest, VOI, was selected at the centre of the specimen to eliminate any edge effects, artefacts and

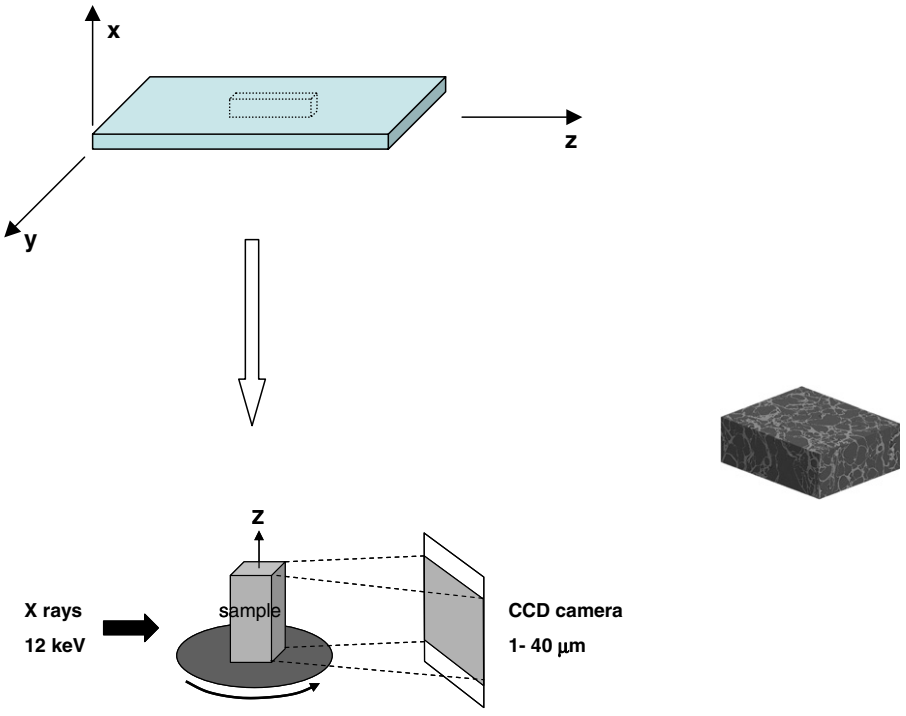

Fig. 1. Schematic view of the experimental set-up of X-ray tomography. Orientation and dimensions of sample B4 ($3 \times 7 \times 9$ mm^3).

damage from sample cutting. Segmentation was performed using a simple threshold. Due to the good contrast of the images, as shown on Fig. 2a, the optimum threshold value was easily determined between the two distinct peaks.

From the binary 3D images, the relative density of the sample was assessed, in an increasing volume, going from the central voxel to the final whole volume, as illustrated by Fig. 2b. In the present case, a representative volume element (RVE) was obtained for 150^3 voxels since the

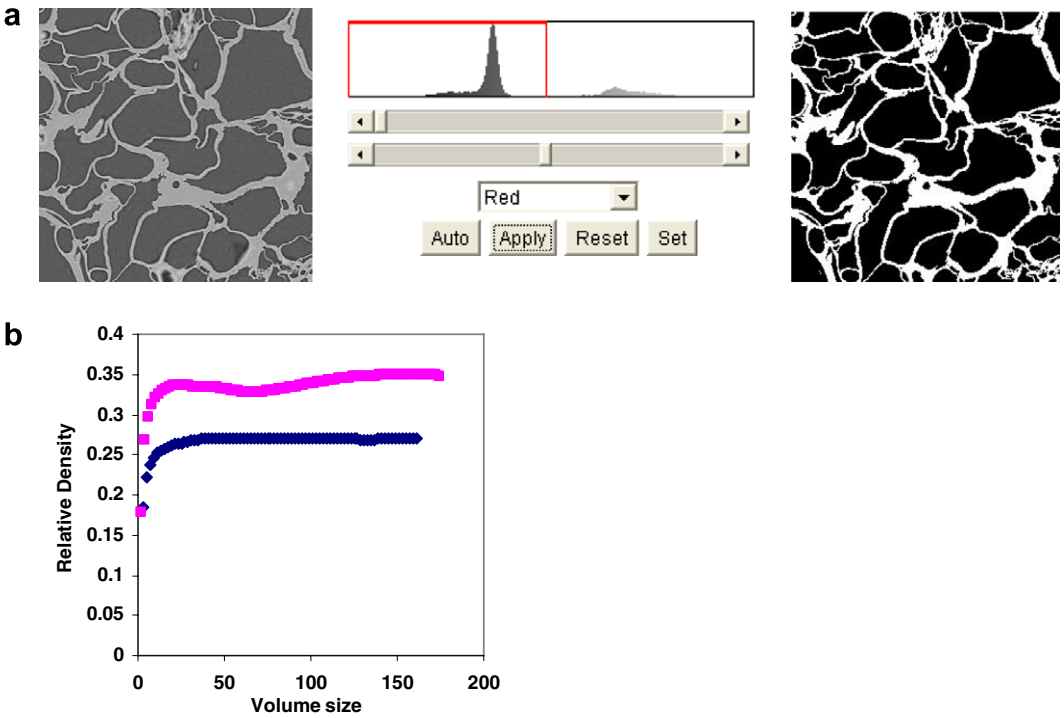

Fig. 2. (a) Two-dimensional images of a 3D tomography sample (B6, (3.5 mm)^2, ESRF-Grenoble) and illustration of thresholding; (b) determination of the representative volume element (RVE) for samples A4 (■) and B4 (◆).

relative density has reached an asymptotic value. Cell size and cell wall thickness distributions and their volumic average values were obtained using 3D granulometry analysis. It was performed by an iteration of erosion/dilation with an octahedral structuring element which size increased at each step, as described in detail by Rouillé, Della Valle, Devaux, Marion, and Dubreil (2005) in the case of 2D images.

Further analysis by labelling of the cavities was performed to determine a connectivity index, noted I_{co}, defined as the ratio of the volume of the largest cavity in comparison with the total void volume. I_{co} may also be considered as the volumic fraction of open cells.

2.4. Mechanical test and dynamic mechanical analysis (DMA)

The mechanical properties of foams were measured for large deformations by three point bending test as described by Lourdin et al. (1995) and those of cell wall material were derived from those measured for films stretching as described in the same work.

Mechanical relaxation measurements were performed on a Dynamic Mechanical Analyser (DMTA MK IV, Rheometric Scientific, USA). Vibration frequency in the dual cantilever bending solicitation mode was 0.2 Hz, the strain was 0.05% and the heating rate 3 °C/min. Strips ($22 \times 10 \times 1$ mm^3) were coated with a silicone-based hydrophobic grease to limit dehydration during experiments at high temperatures. Same measurements with and without a coating of thin plastic film showed that the thin coating of grease had no effect on thermomechanical properties.. The temperature of the glass–rubbery relaxation T_α, associated with the calorimetric glass transition of the material T_g, was determined at the maximum of $\tan\delta = E''/E'$.

3. Results and discussion

3.1. Characterisation of the cellular structure

Typical tomography images of extruded samples show that very different cellular structures are obtained (Fig. 3) whatever the starch composition and processing conditions (moisture content MC, product temperature T_p, shear rate and viscosity at the die outlet) recalled in Table 1. The value of density measured in the preceding study by glass beads displacement is also recalled. It ranges from 109 kg m^{-3} (A1) to 465 kg m^{-3} (C4). For clarity reasons, only 2D sections are presented, although quantitative analysis is performed on the 3D images. Their complexity and diversity are the most striking features and, their contorted appearance suggests that they have been set very quickly, far from a regular polyhedral shape supposed to result from a stabilization process (Warburton et al., 1992). Indeed, some cells appear flattened besides others of circular shape suggesting that the growth of some bubbles has impaired others, at their neighbourhood. At first glance, they range from the coarsest (A1) with large cells and discontinuous walls, suggesting an open cellular structure, to the finest one (A6), with many cells of different size and shape. These differences are not only due to the difference of density since, for instance, sample C1 has a coarse structure, for a density value (274 kg m^{-3}) close to the one of sample A6 (269 kg m^{-3}), which displays a much finer structure. Other samples display both features and can hardly be considered as fine or coarse, which underlines the need for a quantitative analysis.

In Table 1 are also reported the values determined from the analysis of the images. The first feature obtained by tomography is the relative density D^*. It has been checked that the studied volume is representative in order to make sure that the microstructural characteristics are reliable, by measuring D^* in an increasing volume, from one voxel to the final sample size. When D^* does not vary any more, as illustrated in Fig. 2b for samples A4 and B4, a representative volume (RVE) is obtained, which occurred for all samples, except D1 and D3. The size of these two samples (D1 and D3) is likely not large enough to reach a constant density. From D^*, the foam density, noted ρ^*_{AI}, may be directly deduced assuming that density of the amorphous starches $\rho_s = 1405$ kg m^{-3} for a 10% moisture content, the moisture level reached after storage. The values of ρ^*_{AI} were found generally larger than the values previously determined by glass beads displacement ρ^* (Fig. 4). This may be due to the overestimation of the volume measured by glass beads displacement since the value of beads diameter (3 mm) was chosen larger than the extrudate cell size. But this experimental uncertainty (10% according to Della Valle et al., 1997) cannot totally explain the data scattering. The selection of a constant value of ρ_s does not bring more uncertainty, since the density of the cell wall material does not vary by more than 10% according to the values reported by Warburton et al. (1990). The fair correlation is also due to the low value of ρ^*_{AI} predicted for samples D1 and D3, for which the RVE was not reached. Taking these considerations into account, the value considered thereafter for the density of the foams will be the one deduced from D^*, i.e. ρ^*_{AI}, except for D1 and D3 for which ρ^* values will be kept.

Further image analysis by 3D granulometry provides the distribution of cell and cell wall sizes, displayed in Fig. 5, for some samples. They represent the volumic frequency of cells or cell walls which have a size lower than the size of the octahedral structuring element. These curves highlight the different microstructures obtained for close density values (0.24 ± 0.02), according to the starch type and processing conditions, as shown by very distinct cell size distributions. The narrowest one, A6, has a peak at 80μm reflecting a structure more homogeneous than C1 and D1 which have broader distributions, without any noticeable peak. The dispersion displayed for the higher cell sizes (>5 mm) enhances the heterogeneity of these cellular structures. Conversely, B4 presents an intermediate distribution, with a peak at 400 μm (Fig. 5a). Cell wall size distributions display smoother shape indicating sizes or

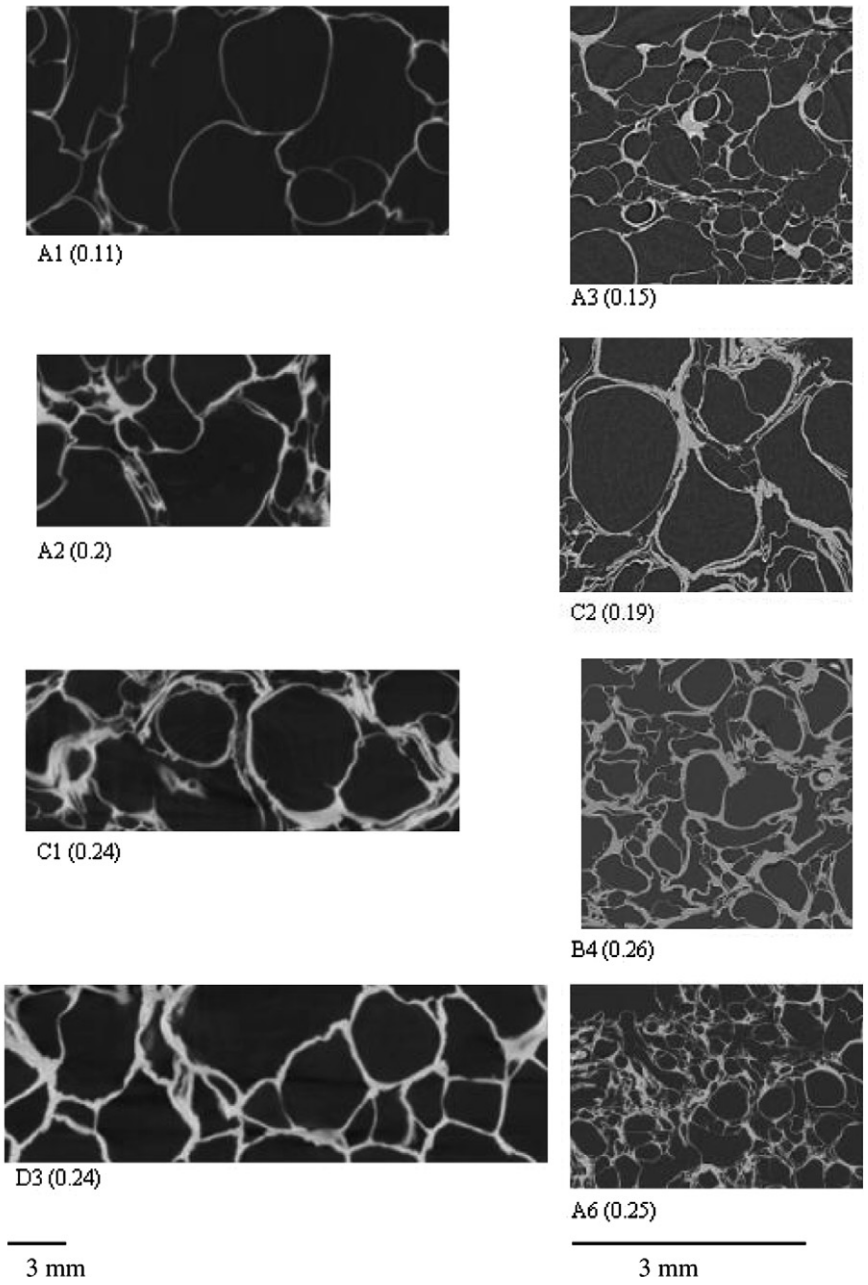

Fig. 3. Typical images obtained by X-ray tomography (ESRF-Grenoble) of samples from left to right, and top to bottom: A1, A3, A2, C2, B4, C1, A6, D3. Relative density D^* is mentioned within brackets. Left column, SPR = 40 μm; right column, SPR = 10 μm. All images are from die cross section (x, y).

thickness lower than 1.5 mm (Fig. 5b). They nearly rank in the same order as the cell size distributions, and display peaks for 40, 80, 320 and 240 μm, respectively for A6, B4, C1 and D2.

Mean cell size (MCS) and mean cell wall thickness (MWT) can be calculated from the distributions and rank above all between 0.22 and 4.84 mm for samples A7 and D1, and between 75 and 595 μm for A7 and D3, respectively (Table 1). The values of MWT are of the same order of magnitude than those encountered by Warburton et al. (1990) and Trater et al. (2005), in the interval [40, 180 μm]. Concerning cell size, Warburton et al. (1990) and Trater et al. (2005) both found MCS values larger than 0.8 mm. This difference with our results may be imparted to the difference of imaging techniques in the first case and to the larger set of processing conditions we explored, in the second. Both features, MCS and MWT, are well linearly correlated ($r^2 = 0.82$). This general trend shows that cellular structures having larger cells also display thicker walls, whatever the foam density (Fig. 6). It appears in contradiction with the current assumption which links foam density to this ratio or to its square value (Gibson & Ashby, 1997). This result confirms the observations of images (Fig. 3) showing that different cellular structures may be obtained for same values of density. This graph also shows that, apart from sample D3, highest moisture conditions

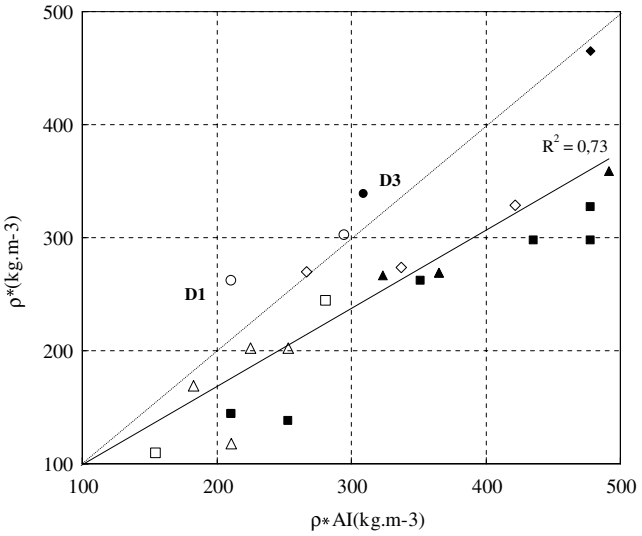

Fig. 4. Comparison of density values found by glass beads and X-ray tomography of starch extruded foams with different amylose content: □ (A, 0.7), △ (B, 0.47), ◇ (C, 0.23), ○ (D, 0). Open and full symbols represent extrusion moisture content 20 (□, △, ◇, ○) and 24% (■, ▲, ◆, ●), respectively. Data from Lourdin et al. (1995). Second line is best fit: $r^2 = 0.73$. Apart for samples D1 and D3, density values determined by tomography are used in the following.

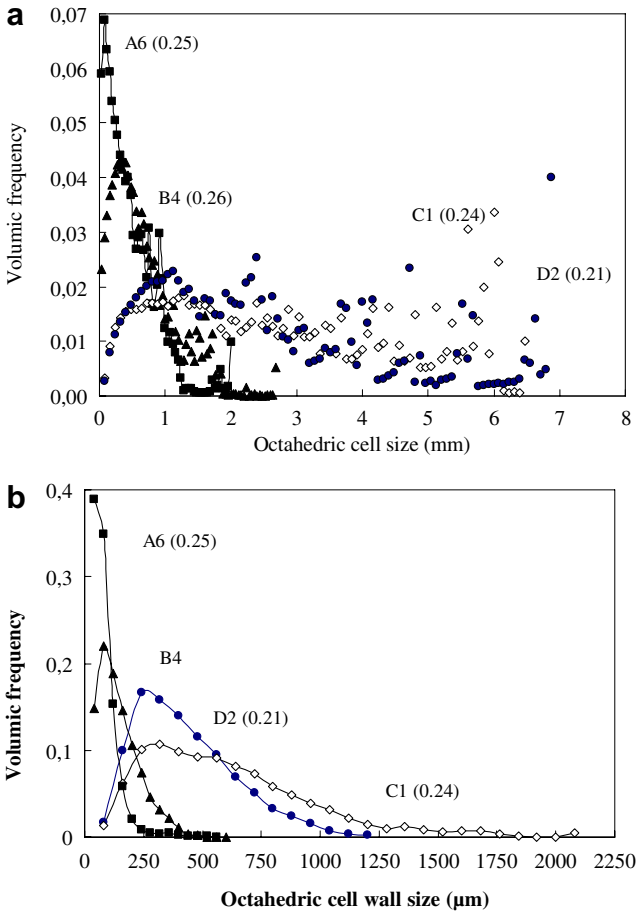

Fig. 5. Examples of cells (a) and cell walls (b) size distributions of starch extruded foams with different amylose content: □ (A), △ (B), ◆ (C), ○ (D). Extrusion moisture content 20% and 24%, open and full symbols, respectively. Relative density is indicated beside sample #.

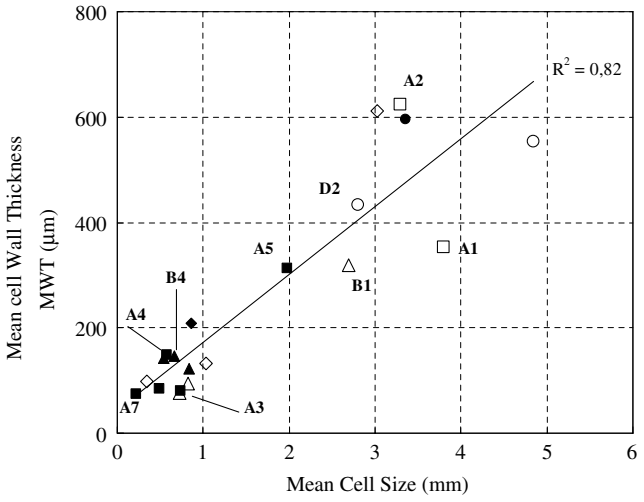

Fig. 6. Variations of mean wall thickness (MWT) as a function of mean cell size (MCS) of starch extruded foams with different amylose content: □ (A), △ (B), ◆ (C), ○ (D). Extrusion moisture content 20% and 24%, open and full symbols respectively. The samples noted are those mentioned in Section 3.3.

during extrusion lead to finest structures (MCS < 2 mm, MWT < 300 µm). The reciprocal is not true since lowest moisture condition may, in some cases, lead to fine cellular structures, as illustrated by samples B2, B3, C2 and C3.

3.2. Relationship between structure and mechanical properties

The preceding analysis has shown that very different cellular structures may be found for the same density value. All samples displayed a fragile mechanical behaviour with rupture in the elastic domain This is why the following focuses on the stress at rupture σ^*. The variations of the normalized values of σ^* have been represented against their relative density on a double-log scale (Fig. 7) allowing fitting to a power law equation suggested by Gibson and Ashby's theory:

$$\frac{\sigma^*}{\sigma_s} \propto \left(\frac{\rho^*}{\rho_s}\right)^n = D^{*n} \quad (1)$$

with σ^* and σ_s, respectively, foam and dense amorphous starch stress at rupture, and $\rho^*/\rho_s = D^*$, the relative density found by image analysis, except for D3 and D1 samples for which D^* was derived from the value ρ^*, as stated before. As expected, data display a large scattering and the fitting with Eq. (1) is not satisfactory ($r^2 = 0.51$). Indeed, in Lourdin et al. (1995), more experimental points led to a better fit ($r^2 = 0.78$, Fig. 4b of this reference). Samples were selected from this previous work in order to emphasize this scattering and explain the remaining lack of fit, i.e. the difference of normalized stress for the same relative density. Every term in Eq. (1) may be inferred for this result. However, the relative density ρ^*/ρ_s has been measured

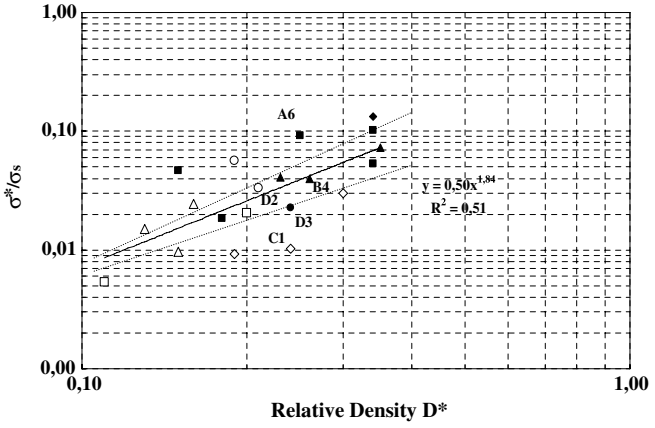

Fig. 7. Variations of normalized fracture stress σ^*/σ_s (data from Lourdin et al., 1995) with density for starch extruded foams with different amylose content selected for X-ray tomography: □ (A), △ (B), ◆ (C), ○ (D). Extrusion moisture content 20% and 24%, open and full symbols, respectively. Samples noted are those for which cell and cell wall distributions are represented in Fig. 5. Continuous line is for the best fit (slope = 1.84, $r^2 = 0.51$). Dotted lines represent the theoretical slope of open cells ($n = 1.5$) and closed cells ($n = 2$).

accurately by X-ray tomography, and even for samples D1 and D3, the order of magnitude of the uncertainty on $\rho*$ does not lead to a significant change in Fig. 7. The values of σ_s were derived from tensile rupture stress measurements, leading to the values (MPa) 38, 46, 53, 60, with increasing amylose content (Lourdin et al., 1995). This ranking was attributed to the higher capacity of linear molecules (amylose) to entangle than the highly branched ones (amylopectin). A difference of cristallinity could not be inferred since it was checked that starch was still amorphous. Recently, these orders of magnitude have been confirmed by those determined by three points bending test (Chanvrier, Colonna, Della Valle, & Lourdin, 2005). So, the dispersion of the variations reported in Fig. 7 could be due to the difference of cellular structure rather than to the terms of Eq. (1).

This hypothesis may be checked by comparing samples A6, B4, C1 and D2 (noted in Fig. 7), which have close density values ($D* = 0.24 \pm 0.02$) but for which the normalized values of stress at rupture vary by a factor of 10. From Fig. 5, it can be deduced that mechanical resistances rank in the opposite way of the spread of cell size and chiefly cell wall thickness distributions. Indeed larger (σ^*/σ_s) values are obtained for low average values of MCS and MWT (A6, B4). Conversely, the most brittle one (C1) has widely spread cell and cell size distributions and high average values of MCS and MWT. At same D^* value, this is also true for sample D3, but cell structural features are not further discussed because RVE was not reached. This explanation may be related to the so-called fracture criterion of the ''weak link'' evidenced by numerical studies (Fazekas et al., 2002): the most spread the wall thickness distribution, the largest is the probability to find a thin wall where the local stresses concentrate and overcome the critical stress. It is tempting to relate it to that given by Liu et al. (2003) who suggested to relate the elastic properties to the microstructure effects by a weak-link regime theory in order to explain the high value of the exponent ($n = 2.54$) by the compliance of amylose regions embedding swollen granules in the cell walls of starch foams made by wheat flour baking. However, this cannot be inferred in our case, since, after extrusion, starch macromolecules are supposed to constitute an homogeneous amorphous matrix.

Another interpretation may refer to possible size effects, as suggested by Onck (2003). A significant decrease of modulus and plastic collapse stress may be found during compression, compared to the bulk values for large specimen, when sample size is less than 6 times the cell size. This could be the case, for instance, for samples C1 and D2, and to a lesser extent D1 and D3, which display large cells as shown by the distribution represented in Fig. 5, since sample thickness for testing was about 1cm. More experiments with specimen of different size from same samples would be required to ascertain this explanation.

A different connectivity of the foam cellular structure, i.e. open or close, could also be responsible for data scattering. The value of exponent ($n = 1.84$), in the interval delineated by the values predicted by Gibson and Ashby in the case of open-cell structures ($n = 1.5$), and closed cell structures ($n = 2$) (dotted lines on the graph), would be in line with this suggestion. However, a high value of the connectivity index, I_{co}, close to 90%, is obtained in all cases, which means that 90% of the void volume is occupied by a connected cavity. That would rather show that, at least from a geometrical point of view, with respect to spatial resolution, extruded starch foams have an open cell structure. This result seems in contradiction with the results of Warburton et al. (1992) and Trater et al. (2005), both suggesting a closed cell structure. Indeed, it is unlikely that thin cell walls would not have been detected by X-ray tomography, for a 10μm resolution. So, we rather believe that this apparent contradiction may be either due to the fact that, in these studies, image analysis has been performed in 2D and that processing conditions were different, leading to different cellular structures. Despite this uncertainty, the term ''cell wall thickness'' is still employed in the following, to characterize a dimensional characteristic of the solid matrix, either cell edge (beam) or wall. So, the explanation for the scattering of the results of mechanical properties likely relates to the cellular structure and suggests that the more dispersed the cell wall size distribution, the less resistant the foam.

3.3. Relationships between processing conditions and cellular structure

Expansion at the die of the extruder can be considered as a succession of phenomena such as bubbles nucleation and growth, coalescence and finally setting, when the melt matrix becomes glassy, possibly after collapse, occurring in

a short time interval (<1 s). All of them influence the cellular structure, and have to be considered when interpreting its formation. They are supposed to be governed by the rheological properties above and close to glass transition. The extrusion variables of the product, such as MC and T_p at the die outlet, affect these material properties and also influence the vaporization. The influence of flow rate is directly taken into account by the local shear rate in the die. Due to these interactions, the influence of these variables is studied separately.

3.3.1. Effect of moisture content

As noticed before, there is an overall trend for starches extruded at higher moisture content to have smaller values of mean cell size (MCS) than those made at lower MC, as illustrated in Fig. 6. This trend is ascertained when considering MCS and MWT values (Table 1) of pairs of samples processed under same temperature and having similar value of shear viscosity at the die outlet, but with distinct values of MC: A1, A2 and B1 extruded at MC = 0.20 clearly display coarser structures than A3, A4 and B4, extruded at MC = 0.24, respectively.

The explanation of the influence of moisture content on cellular structure might be linked to the value of the temperature of glass transition, T_g. As stated by Fan et al. (1994) and Della Valle et al. (1997), for larger MC values, vaporization may have ceased when the matrix is still rubbery (100 °C > T_p > T_g) and then collapses; the bulk extrudate could have shrunk, leading to smaller cells and a larger density, when MC is increased, from 0.2 to 0.24 in our case. However, according to Bizot et al. (1997), the decrease of T_g between these two values of moisture content is certainly low, from 23 to 18 °C, when compared to its overall variation due to moisture loss by vaporization, since T_g is about 60 °C when MC = 0.1. Consequently, the influence of such a tiny difference of ($T_p - T_g$) values can hardly be inferred to explain this huge difference of cellular structure, obtained for the two conditions of moisture. Indeed, the decrease of MCS, by a factor larger than 4, should increase the relative density by a factor of 64 (=4^3), if only collapse phenomenon is implied, instead of an order of magnitude of about 2, in our case. That suggests that there is a strong increase of the apparent volumic number of cells, N_c, simply evaluated by assuming that cells have a spherical shape with a mean diameter value equal to MCS:

$$1 - D^* = N_c \times \frac{4\pi}{3} \times (\mathrm{MCS}/2)^3 \quad (2)$$

This relation, defined according to the model proposed by Fan et al. (1994) to describe expansion, leads to orders of magnitude of N_c varying from 31 cm^{-3}, for A1, to 4000 cm^{-3} for A3, which appears in agreement, at least qualitatively, with the images in Fig. 3. This large increase of N_c can result from the fact that under the same flow conditions, i.e. the same pressure drop in the die of the extruder, more bubbles may be nucleated when water concentration is larger. This interpretation is in agreement with the results obtained by Lee (2001) who found an increase of nucleation ratio by 10, when the concentration of the foaming agent, dissolved CO_2, was increased by 1% in PE matrix foaming by sheet extrusion. When MC is increased, axial expansion, i.e. in the flow direction, would be favoured, as indicated by the values of axial expansion index larger than those of radial expansion (Della Valle et al., 1997). This is also a validation of the hypothesis of Desrumaux et al. (1998) who suggested that, for the same density, two cellular structures, either coarse or fine, may be obtained, according to the type of expansion, radial or axial, respectively, depending on extrusion conditions. The orientation of bubbles in the flow cannot be inferred here, since comparisons are made for samples extruded under similar values of shear rate. So, an increased nucleation, could better explain the finer cellular structure of the starch foam, for larger moisture content, rather than the increased value of ($T_p - T_g$).

3.3.2. Effect of product temperature

Less experimental data are available to study the influence of product temperature at the die. For instance, pairs like (A4, A7) and (B5, B6) cannot be examined in this purpose since viscosity changes with temperature. However, by comparing samples A3 extruded at 163 °C to A5 obtained at 187 °C, respectively, other extrusion variables having close values, it is clear that larger mean cell sizes were obtained at higher temperature, for close values of density (Fig. 6). First, a higher value of T_p could favour the rupture of cell walls by increasing the internal water vapour pressure. This trend is illustrated by the model predictions of Tuladhar and Mackley (2004), and validated by experiments of bubble growth in pentane loaded molten polystyrene. Secondly, the increase of T_p could decrease the resistance of the polymer to elongational flow, as found by Park et al. (1998) for PS extrusion processing using CO_2 as a blowing agent, to manufacture microcellular HIPS. So both phenomena may concur to explain the coarser cellular structure obtained for higher product temperature. Other experiments, for instance by cooling the Rheopac die, would allow to discriminate the effect of product temperature on vaporization from the one on rheological properties. More accurate interpretation would also require to take into account the real value of T_g, which depends on the dehydration kinetics during expansion and the variations of rheological properties close to this transition, which is a good prospect for improving the capacity of actual models for predicting expansion (Alavi et al., 2003; Fan et al., 1994).

3.3.3. The role of rheological properties and amylose content

As expected, the steady-shear viscosity of the molten material limits overall expansion, provided that other variables (MC, T_p, amylose content) are kept constant. This trend is well illustrated by the increase of density of sample A7 by a factor of 2, when compared to sample A5 (Table 1), when viscosity is increased by the same

factor, resulting from a decrease of shear rate from 162 to 12 s^{-1}. This result seems in complete agreement with the model of the growth of a vapour bubble in a viscous fluid, on which are generally based most models for expansion (Amon & Denson, 1984). Viscosity acts like a brake on the growth of the bubbles, and the quicker they grow and water evaporates, the sooner the cellular structure is set. However, when viscosity increases, i.e. when shear rate is decreased, MCS decreases by a factor close to 10, so, according to Eq. (2), the apparent volumic number of cells, N_c, should increase significantly, since D^* is only increased by a factor of about 2. Hence, the decrease of MCS cannot be explained only by the limiting role of viscosity on bubble growth. As shown by the results of Lee (2001), nucleation is rather known to increase when shear rate is increased, because of the increased pressure drop (Gendron et al., 2002; Han et al., 2002). So, the decrease of N_c and the increase of MCS for larger shear rates can neither be explained by nucleation. This result could rather be due to an increase of coalescence, as suggested by Park et al. (1998). Indeed, for faster bubble growth, the strain rate is increased, and, as mentioned before for higher temperature (see Section 3.3.2), the resulting decrease of resistance of the melt to elongational flow favours wall rupture.

The importance of the elongational behaviour of molten materials is well known for polymer foaming or film blowing (Dealy & Wissbrun, 1989), and it is interesting to ascertain its possible influence on the molten starch foaming. This material property could explain why, as already observed by Della Valle et al. (1997), for the same extrusion variables and similar values of shear viscosity, samples having decreasing amylose content (A1, B1, D2) display increasing density, from 0.11 to 0.21 (see Table 1). However, data on elongational viscosity of molten starchy products are scarce and make difficult the comparison of the behaviour of starches from different botanical origin. The apparent elongational viscosity of plasticized wheat starch has been shown to follow a strain rate thinning behaviour (Martin, Avérous, & Della Valle, 2003). Since this variable also reflects the elastic properties, it may be useful to determine, by DMA, the elastic modulus E' of the thermal moulded samples, assumed to behave like molten starch before die expansion. Care has to be taken when considering modulus variations at such high temperature, because of possible evaporation during testing, but, as shown later on, this result is qualitatively acceptable due to the large difference obtained between E' values, more than one decade. The tanδ peak marks the temperature of the principal relaxation $T_\alpha = 137 \pm 3$ °C, linked to the glass transition, for all starches except for starch containing 70% amylose (Fig. 8a). The amplitude of this peak decreases with the increase of amylose content. The maximum drop of E' is obtained at T_α, except for starch containing 70% amylose, which shows a regular decrease (Fig. 8b). Differences of E' values at temperatures lower than 110 °C, i.e. in the glassy domain, are not considered here, but for $T > T_\alpha$, in the rubbery domain, they clearly rank according to the amylose content. Similar result has already been observed by performing frequency sweeps at high temperature on samples of plasticized starches from different botanical origin (Della Valle, Buleon, Carreau, Lavoie, & Vergnes, 1998). It confirmed that this trend could be attributed to the larger ability of the linear macromolecules (amylose) to entangle and thus restrict mobility, than the highly branched one (amylopectin) supposed to adopt a more compact conformation (Della Valle et al., 1996). Assuming that the material tested by DMA is representative of the matrix during expansion, it might be suggested, in agreement with the results obtained by Chanvrier (2004), that the resistance to elongational flow, i.e. elongational viscosity, ranks in the same way as E' values. This result might then explain why samples containing less amylose are less expanded. Indeed, lower resistance of the melt to elongational flow favours coalescence within these materials, upon cooling in the vicinity of Tα, just before foam setting, hence leading to a larger density. At larger temperatures, the bubble growth is favoured by low viscosity, as reflected by the influence of shear viscosity but, for lower temperature, closer to T_α and foam setting, lower values of elongational viscosity would finally contribute to reduce the void volume. The determination of the contribution of

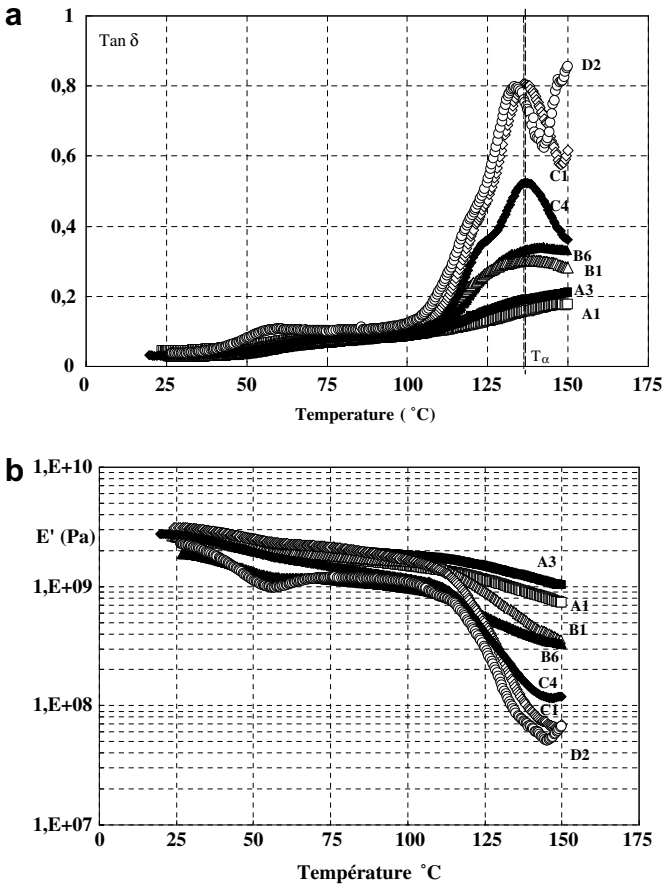

Fig. 8. Variations of tanδ (a) and elastic modulus E' (b) of moulded starch foams samples (MC = 0.09) with temperature.

elongational properties, compared with the shear viscosity, remains an issue for the control of the expansion mechanisms of starch materials.

4. Conclusion

X-ray tomography, coupled with 3D image analysis, appears a very efficient tool for 3D quantitative description of the cellular structure, to determine the distributions of cell size and cell wall thickness, their volumic mean values and relative density. The main findings are that for the same density value, very different cellular structures may be obtained according to the extrusion variables and product composition, here water or amylose contents. Coarser structures, characterized by a high mean cell size and widely spread cell size distribution, also display thick cell walls. For the same density, these foams have less mechanical resistance than more homogeneous ones with finer structure characterized by lower mean cell size and cell wall thickness values. Such fine, but denser structures, can be obtained either by increasing moisture content during extrusion which can be explained by an enhanced nucleation in the die, or by decreasing product temperature because of $(T_p - T_g)$ increase and foam setting delay. Finally, it was found that increasing amylose content also leads to such cellular structures, which could be explained by taking into account the role of elongational properties, in a range of temperature of the rubbery domain close to glass transition.

These interpretations are mere trends and should be ascertained by computing the contribution of each factor, since they largely interact and that requires the improvement of actual expansion models. Of course, an in situ tomography study of the starch foam expansion would allow to address all these issues. Meanwhile, a better understanding of the mechanisms of gas cell expansion also requires the measurement of elongational viscosity of starch melts and its comparison with the viscoelastic properties at temperature just above T_g. In complement, comparison of the mechanical properties of foams having different cellular structures, eventually using mechanical modelling approaches, would open prospects for the design of extruded products with desired textural properties.

Acknowledgments

The authors are grateful to Roselyne Desirest (BIA) for careful samples assessment and Elodie Boller (ESRF) for her help in the X-ray tomography experiments. This work has been carried out in the frame of CANAL-Salve program from the French Ministry of Research within which partners contribution is gratefully acknowledged and Dr. Chantal David (SCC) is specially thanked for helpful discussions.

References

Alavi, S. H., Rizvi, S. S. H., & Harriott, P. (2003). Process dynamics of starch based cellular foams produced by supercritical fluid extrusion. II: numerical simulation and experimental evaluation. *Food Research International, 36*, 321–330.

Amon, M., & Denson, C. D. (1984). A study of the dynamics of the growth of closely spaced spherical bubbles. *Polymer Engineering and Science, 24*, 1026–1034.

Babin, P., Della Valle, G., Chiron, H., Cloetens, P., Hoszowska, J., Pernot, P., et al. (2006). Fast X-ray tomography analysis of bubble growth and foam setting during breadmaking. *Journal of Cereal Science, 43*, 393–397.

Bizot, H., Le Bail, P., Leroux, B., Davy, J., Roger, P., & Buléon, A. (1997). Calorimetric evaluation of the glass transition in hydrated, linear and branched polyanhydroglucose compounds. *Carbohydrate Polymers, 32*, 33–50.

Chanvrier, H. (2004). Materiaux a base de biopolymers du maïs: elaboration et comportment mecanique. Universite de Nantes. Ph.D. Thesis, 164p.

Chanvrier, H., Colonna, P., Della Valle, G., & Lourdin, D. (2005). Structure and mechanical behaviour of corn flour and starch-zein based materials in the glassy state. *Carbohydrate Polymers, 59*(1), 109–119.

Dealy, J. M., & Wissbrun, K. F. (1989). *Melt rheology and its role in plastics processing*. New York: Van Nostrand Reinhold, 665p.

Della Valle, G., Buleon, A., Carreau, P., Lavoie, P.-A., & Vergnes, B. (1998). Relationship between structure and viscoelastic properties of plasticized starches. *Journal of Rheology, 42*, 507–525.

Della Valle, G., Colonna, P., Patria, A., & Vergnes, B. (1996). Influence of amylose content on the viscous behaviour of low hydrated molten starches. *Journal of Rheology, 40*(3), 347–362.

Della Valle, G., Vergnes, B., Colonna, P., & Patria, A. (1997). Relations between rheological properties of molten starches and their expansion behaviour in extrusion. *Journal of Food Engineering, 31*, 277–296.

Desrumaux, A., Bouvier, J. M., & Burri, J. (1998). Corn grits particle size and distribution effects on the characteristics of expanded extrudates. *Journal of Food Sciences, 63*, 857–863.

Falcone, P. M., Baiano, A., Zanini, F., Mancini, L., Tromba, G., Dreossi, D., et al. (2005). 3D quantitative analysis of bread crumb by X-ray tomography. *Journal of Food Science, 70*, 265–272.

Falcone, P. M., Baiano, A., Zanini, F., Mancini, L., Tromba, G., Montanari, F., et al. (2004). A novel approach to the study of bread prorous structure: phase-contrast X-ray microtomography. *Journal of Food Science, 69*, 38–43.

Fan, J., Mitchell, J. R., & Blanshard, J. M. V. (1994). A computer simulation of the dynamics of bubble growth and shrinkage during extrudate expansion. *Journal of Food Engineering, 23*, 337–356.

Fazekas, A., Dendievel, R., Salvo, L., & Brechet, Y. (2002). Effect of microstructural topology upon the stiffness and strength of 2D cellular structures. *International Journal of Mechanical Sciences, 44*, 2047–2066.

Gendron, R., Huneault, M., Tatibouët, J., & Vachon, C. (2002). Foam extrusion of polystyrene blown with HFC-134a. *Cellular Polymers, 21*, 315–341.

Gibson, L. J., & Ashby, M. F. (1997). *Cellular solids* (Second ed.). Cambridge, UK: Cambridge University Press.

Han, X., Koelling, K. W., Tomasko, D. L., & Lee, L. J. (2002). Continuous microcellular polystyrene foam extrusion with supercritical CO_2. *Polymer Engineering and Science, 42*, 2094–2106.

Hayter, A. L., Smith, A. C., & Richmond, P. (1986). The mechanical properties of extruded food foams. *Journal of Material Science, 21*, 3729–3736.

Kokini, J. L., Chang, C. N., & Lai, L. S. (1992). The role of rheological properties on extrudate expansion. In J. L. Kokini, C. T. Ho, & M. V. Karwe (Eds.), *Food Extrusion, Science and Technology* (pp. 631–652). New York: Marcel Dekker.

Lee, S. T. (2001). Nucleation in foam extrusion. *Journal of Cellular Plastics, 37*, 221–230.

Lim, K. S. & Barigou, M. (20024). X-ray computed tomography of cellular food products. *Food Research International, 37*, 1001–1012.

Liu, Z., Chuah, C. S. L., & Scanlon, M. G. (2003). Compressive elastic modulus and its relationship to thestructure of a hydrated starch foam. *Acta Materialia, 51*, 365–371.

Liu, Z., & Scanlon, M. G. (2003). Scaling Young's modulus of cellular solids. *Journal of Material Science Letters, 22*, 547–548.

Lourdin, D., Della Valle, G., & Colonna, P. (1995). Influence of amylose content on starch films and foam. *Carbohydrate Polymers, 27*, 261–270.

Maire, E., Fazekas, A., Salvo, L., Dendievel, R., Youssef, S., Cloetens, P., et al. (2003). X-ray tomography applied to the characterization of cellular materials. Related Finite Element modeling problems. *Composite Science and Technology, 63*, 2431–2443.

Martin, O., Avérous, L., & Della Valle, G. (2003). In line determination of plasticized wheat starch viscous behaviour: impact of processing. *Carbohydrate Polymers, 53*, 169–182.

Onck, P. R. (2003). Scale effects in cellular materials. *MRS Bulletin*, 279–283.

Park, C. B., Behravesh, A. H., & Venter, R. D. (1998). Low density microcellular foam processing in extrusion using CO_2. *Polymer Engineering and Science, 38*, 1812–1823.

Rouillé, J., Della Valle, G., Devaux, M. F., Marion, D., & Dubreil, L. (2005). French bread loaf volume variations and digital image analysis of crumb grain changes induced by the minor components of wheat flour. *Cereal Chem., 82*, 20–27.

Trater, M., Alavi, S. & Rizvi, S.S.H. Use of non invasive X-ray microtomography for characterizing microstructure of extrudd biopolymer foams. *Food Research International, 38*, 709–719.

Tuladhar, T. R., & Mackley, M. R. (2004). Experimental observations and modelling relating to foaming and bubble growth from pentane loaded poystyrene melts. *Chemical Engineering Science, 59*, 5997–6014.

Vergnes, B., Della Valle, G., & Tayeb, J. (1993). A specific slit die rheometer for extruded starchy products. Design, validation and application to maize starch. *Rheology Acta, 32*, 465–476.

Warburton, S. C., Donald, A. M., & Smith, A. C. (1990). The deformation of brittle starch foams. *Journal of Material Science, 25*, 4001–4007.

Warburton, S. C., Donald, A. M., & Smith, A. C. (1992). Structure and mechanical properties of brittle starch foams. *Journal of Material Science, 27*, 1469–1474.

Whitworth, M., & Alava, J. M. (2004). Non destructive imaging of bread and cake structure during baking. In S. P. Cauvain, S. S. Salmon, & L. S. Young (Eds.), *Using cereal science and technology for the benefit of consumers* (pp. 221–231). Cambridge, UK: Woodhead Publishing.